

Modelling of turbulent impurity transport in fusion edge plasmas using measured and calculated ionization cross sections

Alexander Kendl

*Institute for Ion Physics and Applied Physics, University of Innsbruck,
Association Euratom-ÖAW, Technikerstr. 25, 6020 Innsbruck, Austria*

Abstract

Turbulent transport of trace impurities in the edge and scrape-off-layer of tokamak fusion plasmas is modelled by three dimensional electromagnetic gyrofluid computations including evolution of plasma profile gradients. The source function of impurity ions is dynamically computed from pre-determined measured and calculated electron impact ionization cross section data. The simulations describe the generation and further passive turbulent $E \times B$ advection of the impurities by intermittent fluctuations and coherent filamentary structures (blobs) across the scrape-off-layer.

*This is a preprint version (with reduced figure quality) of publication
International Journal of Mass Spectrometry **365/366**, 106-113 (2014)
in an honorary issue dedicated to the 70th birthday of Tilmann Märk.*

I. INTRODUCTION

Magnetically confined plasmas for fusion research would ideally be composed of electrons and only the main hydrogen ion species, which usually are either simply protons or deuterium ions for most present experiments, or consist of a deuterium and tritium ion fuel mixture and helium ions as their fusion product in burning plasmas. The electron-hydrogen plasma unavoidably gets into contact with wall materials, both (preferentially) in designated strike areas in the divertor region, and also (strongly undesired) on the first wall surrounding the bulk plasmas.

Plasma-wall interaction processes in tokamak fusion experiments [1–4] can generate various neutral and ionized atoms and molecules, which may penetrate into and profoundly disturb the main plasma, and also can lead to unfavourable co-deposition of materials and composites (e.g. of tritiated hydrocarbons) in other areas of the vessel. Detailed knowledge of atomic and molecular interactions in the edge of tokamaks and of the transport of impurities is therefore of considerable interest for understanding and modelling of fusion plasmas.

The major cross-field transport mechanism of particles and energy in magnetized fusion plasmas is turbulent fluid-like convection by wave-like fluctuating electric fields $\mathbf{E}(\mathbf{x}, t)$ acting on the plasma through the $\mathbf{E} \times \mathbf{B}$ drift velocity in a background magnetic field [5–12]. The relevant drift wave turbulence micro-scales in tokamak edge plasmas are in the order of sub-mm spatial vortex structures in the MHz frequency range, but are further closely coupled to macro-scale zonal flow structures [13] and meso-scale instabilities like edge-localized modes [14] and magnetic islands.

Once impurities, which are born at the outer edge of the plasma region, are ionized by electron impact or other processes, they are also subjected to the turbulent $\mathbf{E} \times \mathbf{B}$ advection and may as a consequence be efficiently transported further across the field and radially inwards.

In this work we study the passive transport of fusion relevant trace impurity ions by means of multi-species edge turbulence computations, which include dynamical electron-impact ionization in fluctuating filamentary plasma structures as a source for impurity ions in the scrape-off-layer region of a tokamak.

II. GYROFLUID TURBULENCE MODEL INCLUDING IMPURITIES

The present flux-driven 3-d multi-species isothermal gyrofluid turbulence model includes evolution of density profile gradients and dynamically couples the edge pedestal region with a limiter bounded scrape-off layer (SOL).

The model is based on the local gyrofluid electromagnetic model ‘‘GEM3’’ by Scott [10, 15] and the SOL (limiter) model by Ribeiro & Scott [16, 17], applying globally consistent geometry [18] with a shifted metric treatment of the coordinates [19]. An Arakawa-Karniadakis numerical scheme [20–22] is used for the computations. The present multi-species code (‘‘TOEFL’’) has been cross-verified in the local cold-ion limit with the tokamak edge turbulence standard benchmark case of Falchetto et al. [23], and with the results of finite Larmor radius (warm ion) SOL blob simulations of Madsen [24].

In the local (delta-f) isothermal multi-species gyrofluid model [15] the normalised equations for the fluctuating gyrocenter densities n_s , including evolution of the profile gradients, are

$$\partial_t n_s + [\phi_s, n_s] = \nabla_{\parallel} v_{s\parallel} + \kappa(\phi_s + \tau_s n_s) + S_{ns} \quad (1)$$

where the index s denotes the species with $s \in (e, i)$ for the main plasma components (electrons and here main deuterium ions) plus one or more additional ion species ($s \equiv z$). The parallel velocities $v_{\parallel s}$ and the vector potential A_{\parallel} evolve according to

$$\hat{\beta} \partial_t A_{\parallel} + \hat{\mu}_s (\partial_t v_{s\parallel} + [\phi_s, v_{s\parallel}]) = -\nabla_{\parallel} (\phi_s + \tau_s n_s) + 2\hat{\mu}_s \tau_s \kappa(v_{s\parallel}) - \hat{C} J_{\parallel}. \quad (2)$$

The gyrocenter densities are coupled to the electrostatic potential ϕ by the local gyrofluid polarisation equation

$$\sum_s a_s \left[\Gamma_{1s} n_s + \frac{1}{\tau_s} (\Gamma_{0s} - 1) \phi \right] = 0 \quad (3)$$

and the velocities and current to the parallel component of the fluctuating vector potential by Ampere’s equation

$$\nabla_{\perp}^2 A_{\parallel} = J_{\parallel} = \sum_s a_s v_{s\parallel}. \quad (4)$$

where the gyro-averaging operators in Padé approximation are defined by $\Gamma_{0s} = (1 + b_s)^{-1}$ and $\Gamma_{1s} = (1 + (1/2)b_s)^{-1}$ with $b_s = \tau_s \mu_s \nabla_{\perp}^2$.

Spatial scales are normalised by the drift scale $\rho_0 = \sqrt{T_e m_i} / (eB)$, where T_e is a reference electron temperature, m_i is the ion mass, and B is the magnetic field strength. Time scales

are normalized by c_s/L_\perp , where $c_s = \sqrt{T_e/m_i}$, and L_\perp is the generalized profile gradient scale length.

The parameter $a_s = Z_s n_{s0}/n_{e0}$ describes the ratio of species normalising background densities n_{s0} to the reference density n_{e0} (here usually taken at mid-pedestal value) for species with charge state Z_s . The mass ratio is given by $\mu_s = m_s/(Z_s m_i)$, and the (constant) temperature ratio by $\tau_s = T_s/(Z_s T_e)$.

For electrons $a_e = \tau_e = -1$, $\mu_e \approx 0$, and finite Larmor radius (FLR) effects are neglected so that $b_e \equiv 0$. The gyro-screened potentials acting on the ions are given by $\phi_s = \Gamma_s \phi$.

Defining $\hat{\epsilon} = (qR/L_\perp)^2$ as the squared ratio between parallel length scale $L_\parallel = qR$ (for given safety factor q and torus radius R) and perpendicular scale L_\perp , the main parameters are $\hat{\mu}_s = \mu_s \hat{\epsilon}$, $\hat{\beta} = (n_{e0} T_e / B_0^2) \hat{\epsilon}$, and $\hat{C} = 0.51(m_e \nu_e L_\perp / c_{s0}) \hat{\epsilon}$. Quasi-neutrality implies $a_i = 1 - a_z$. If gradients were to be fixed with $g_s \equiv \partial_x n_{s0}$ (alternatively to the present fixed source flux computations) then also $g_i = (1 - a_z g_z)/(1 - a_z)$ needs to be satisfied. For flux-driven computations the sources have to obey quasi-neutrality and ensure vorticity free injection.

The nonlinear advection terms in equations (1) and (2) are expressed through Poisson brackets using the notation $[a, b] = (\partial_x a)(\partial_y b) - (\partial_y a)(\partial_x b)$. Normal and geodesic components of the magnetic curvature enter the compressional effect on vortices due to magnetic field inhomogeneity by $\kappa = \kappa_y \partial_y + \kappa_x \partial_x$ where the curvature components in toroidal geometry are a function of the poloidal angle θ mapped onto the parallel coordinate z . For a circular torus $\kappa_y \equiv \kappa_0 \cos(\theta)$ and $\kappa_x \equiv \kappa_0 \sin(\theta)$ when $\theta = 0$ is defined at the outboard midplane.

The term S_{ns} on the right hand side of the density equation (1) describes particle sources and sinks. For electrons a constant core flux driven density source is applied, which is localized around the inside (left) radial computational boundary at r_0 following a narrow Gaussian profile $S_{ne} \sim s_e(r - r_0)$. The corresponding vorticity free source function for warm ions is FLR corrected by $s_i = s_e - (1/2)\tau_i \nabla^2 s_e$.

The source (and sink) term S_{nz} for impurity ions is here dynamically set by ionization processes of a neutral impurity cloud, as described in the next section. For quasi-neutral non-trace impurities the electron density has to include a corresponding ionization source term. In the following we however will consider only trace impurities ($a_z \ll 1$) which do not enter into polarization or react back on the convecting main plasma turbulence.

For the moment we also neglect recombination processes. Vorticity free Dirichlet conditions are applied for all species on the outer (right) computational boundary. In ref. [34] the necessity of using consistent energy sources has been stressed for cases when temperature fluctuations are dynamically evolved in addition to density fluctuations. Here we presently focus on an isothermal model, so we do not encounter difficulties due to spurious thermal energy sources.

The present local model assumes small density fluctuations on a constant background to approximate $\ln n_s \approx n_s/n_{s0} \equiv n_s$, and can not capture spatially localised non-trace impurity effects, like back-reaction of impurity aggregation on the vortex or zonal flow fine structure. A full-f density (“global”) model would have to account for nonlinear (nonlocal) polarisation via

$$\sum_s [q_s \Gamma_{1s} n_s + \nabla \cdot (n_s \mu_s \nabla) \phi] = 0. \quad (5)$$

For passively advected trace impurities ($a_z \ll 1$) we can however consistently solve the global gyrocenter density equation

$$\partial_t n_z + [\phi_z, n_z] = \nabla_{||} (n_z v_{z||}) + n_z \kappa(\phi_z) + \tau_z \kappa(n_z) + S_{nz} \quad (6)$$

and obtain the actual trace impurity particle density including nonlinear polarisation by

$$N_z = \Gamma_{1z} n_z + \frac{\mu_z}{q_z} \nabla \cdot (n_z \nabla) \phi. \quad (7)$$

In the present simulations the local equations (1), (2), (3), (4) are used for the main plasma species, and the global model eq. (6) to evolve the trace impurities.

III. DYNAMICAL SOURCE OF IMPURITY IONS

For simulations of trace impurity ion transport in a turbulent edge plasma, usually either a cloud of impurity ions is initialized at a single point in time with a given spatial distribution on a turbulent background plasma, or a constant source of impurities is applied at each time step. The evolution of impurities by nonlinear $E \times B$ advection is then further followed to study its migration and inward transport, like in fluid computations of edge turbulence of e.g. refs. [25–28].

Here we extend such previous approaches by applying a edge-SOL coupled model with global profile gradient evolution, and in addition by including a time dependent impurity ion source dynamically computed from ionization processes depending on the local fluctuating electron density and temperature. A localized and (on the turbulent time scale) stationary neutral impurity cloud acts as the background source.

In the following we exemplarily consider electron impact ionization as the main ionization channel. The temperature dependent reaction rates $R(T) = \langle \sigma v \rangle$ of the ionization processes are (pre-)computed from fit functions of measured or calculated ionization cross sections $\sigma(E)$.

The ionization source function $S_{nz} = \nu_{ion} n_e$ in eq. (6) is determined by the product of the ionization frequency ν_{ion} with the spatio-temporally fluctuating electron density $n_e(\mathbf{x}, t)$. The ionization frequency is determined by the neutral background gas density N_n and by the reaction rate $R(T)$ through $\nu_{ion} = N_n(r) R(T)$. The neutral density is here assumed to be constant in time and radially localized, described by a Gaussian radial distribution $N_n(r) = N_{n0} \exp[-(r - r_n)^2 / \Delta_n^2]$ with half width Δ_n around a position r_n within the scrape-off-layer.

The electron impact ionization reaction rate is given by

$$R(T) = \langle \sigma v \rangle = \int dE f(E, T) \sigma(E) v = R_0 T^{-3/2} \int dE E \exp\left(-\frac{E}{T}\right) \sigma(E). \quad (8)$$

The distribution function $f(E, T)$ is here assumed to be Maxwellian for a given thermalized electron temperature T . The prefactor R_0 absorbs all the constants of the Maxwell-Boltzmann distribution and the drift scale normalization of the gyrofluid model.

The present isothermal turbulence model does not actually dynamically evolve the electron temperature. From six-moment gyrofluid equations like in ref. [14] we can infer that

the turbulent fluctuations of the electron temperature relatively closely follow the spatio-temporal structure of the fluctuating electron density. We can thus here approximately use a proportionality relation $T(\mathbf{x}, t) = (T_0/n_{e0}) n_e(\mathbf{x}, t)$ to dynamically compute the temperature entering in the ionization rate $R(T)$.

The ionization cross section $\sigma(E)$ in eq. (8) may most conveniently with sufficient accuracy be supplied in the form of fitting functions of calculated or experimentally determined data.

For theoretical calculations of both single atoms and also complex molecules, the semi-classical Deutsch-Märk (DM) formalism [29–31] for electron impact ionization has been developed by Hans Deutsch and Tilmann Märk in the late 1980s to 1990s with further following refinements and generalizations. The DM method is based on a semi-empirical combination of the binary encounter approximation and the Born-Bethe approximation, and has been proven of considerable practical value.

Here we are specifically interested in ionization cross sections of impurity atoms and molecules relevant to fusion edge plasmas. The impurities usually result from plasma-wall interaction processes. For carbon (or carbon fiber composite) tiled walls or divertor plates, a multitude of different hydrocarbon molecules and ions can form. Beryllium is intended to be used for covering the first wall of the main chamber in ITER. Tungsten has recently received growing interest as a potential general tokamak first wall material, and is going to be used on strike point areas in the ITER divertor.

Electron impact ionization cross sections of beryllium and beryllium hydrides have recently been calculated by the DM-formalism and the Binary-Encounter-Bethe (BEB) formalism in ref. [35]. The theoretical results have been cast into fit functions of the form

$$\sigma(E) = \left(\frac{a_1}{E}\right) \left[1 - \left(\frac{I}{E}\right)\right]^{a_2} \left[\ln\left(\frac{E}{I}\right) + a_3 + a_4\left(\frac{I}{E}\right)\right] \quad (9)$$

which is given units of 10^{-16} cm². Here I is the threshold energy and a_i are the fit coefficients. For e.g. single ionization of gas-phase Be, the coefficients $a_1 = 70.3260$, $a_2 = 1.2341$, $a_3 = 1.7644$ and $a_4 = -0.7628$ with $I = 9.32$ eV have been obtained as fit to the DM theory [35].

In contrast to beryllium, a comprehensive experimental data base of measured electron impact ionization cross section data of hydrocarbon molecules and ions has meanwhile been established. Many such fusion relevant experimental atomic and molecular data have over the last decade been obtained in the lab of Tilmann Märk, like electron impact cross sections of methane [36], acetylene [37], ethylene [38] or propene [39]. These measured hydrocarbon

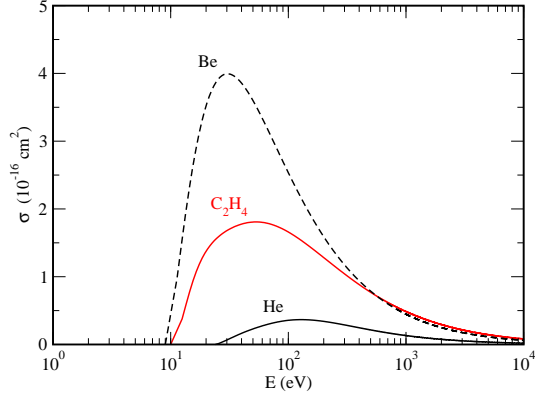


FIG. 1: Fit functions for the electron impact ionization cross sections of Be (calculated by the Deutsch-Märk formalism [35]), C_2H_4 (fitted to experimental data of Märk et al. [40]) and He [46].

cross section data have recently been re-assessed by Huber et al. in ref. [40] and cast into fit functions of the format used in the HYDKIN [41, 42] cross section data base:

$$\sigma(E) = \frac{1}{EI} \left[a \ln \left(\frac{E}{I} \right) + \sum_{j=1}^N b_j \left(1 - \frac{I}{E} \right)^j \right] \quad (10)$$

in units of 10^{-13} cm^2 . For example, the fitting parameters for the measured partial ionization cross section of ethylene for the channel $e + C_2H_4 \rightarrow C_2H_4^+ + 2e$ have been obtained as $a = 1.5525$, $b_1 = -1.4257$, $b_2 = 0.3340$, $b_3 = 0.1928$, $b_4 = -3.8585$ and $b_5 = 2.7727$ for $I = 10.51 \text{ eV}$.

Impurities in fusion edge plasmas may not only arise from unwanted chemical erosion of wall materials, but can also be injected on purpose into the edge plasma, for example as a means to enhance radiative energy losses (and thus reduce heat fluxes) in front of the divertor by gas seeding [43], or for localized detection of light emissions by fast helium gas puff imaging experiments on edge turbulence [44].

Electron impact ionization cross sections for helium are, in contrast to the previous examples, long known with acceptable accuracy. The approximate analytic fitting formula in the form used also above for eq. 10 has been introduced by Bell et al. in ref. [45]. Here we use more recent data for electron impact ionization of helium by Ralchenko et al. [46], where e.g. the parameters for single ionization of He I from the 1^1s state are given as $a = 0.5857$, $b_1 = -0.4457$, $b_2 = 0.7680$, $b_3 = -2.521$, $b_4 = 3.317$ and $b_5 = 0$ with $I = 24.6 \text{ eV}$.

These fit formulas for $\sigma(E)$ are shown in fig. 1 and are in the following used to determine reaction rates $R(T)$ for the impurity ion source terms in plasma edge turbulence simulations.

IV. IONIZATION AND CONVECTION OF BE BY RADIALY PROPAGATING BLOBS

Cross-field transport in the scrape-off-layer of fusion plasmas is predominantly carried by intermittent radially propagating filamentary structures, often termed “blobs”, which originate from a region around the separatrix and are mostly sheared off from edge turbulence vortices and flows in the outer closed field line region [47–54].

The fully turbulent system including both the closed field line edge pedestal region and the SOL with turbulent self-generated blob-like transport will be considered in the next section.

Here we first focus on the ionization and further nonlinear advection of a solitary blob structure on an initially neutral cloud within the SOL. The present computations are fully 3-d including drift and FLR effects.

For the blob initial condition we specify a quasi-neutral Gaussian density perturbation (with half width $6 \rho_s$), accelerating and moving through a radially localised cloud of impurities.

The FLR and warm ion effect for $\tau_i = 1$ have previously been found to induce a pronounced up-down asymmetry on the radial blob propagation [24], whereas 3-d drift effect (with finite $\hat{\epsilon}$) have been reported to lead to a combination of both radial blob and perpendicular drift wave motion [52, 53].

The plasma parameters for the blob computations used here are $\sqrt{\hat{\epsilon}} = (qR/L_\perp) = 316$, $\hat{\beta} = 1$, $\hat{C} = 3.5$, $\tau_i = 1$, and $\kappa_0 = 0.05$, which reflect typical values found in tokamak edge plasmas. As trace impurity species ($a_z = 0$) we exemplarily choose beryllium, and here for simplicity investigate only the ionization into and dynamics of the singly ionized charge state. In principle, multiple equations for either different impurity species or for different charge states of one specific impurity species could straightforwardly be implemented in the gyrofluid code. These refinements will be considered in future work.

We assume that the beryllium ions are colder than the main ions or electrons and set $\tau_z = 0$, and have $\mu_z = 4.5$ in relation to deuterium mass. As numerical parameters, we use a box size of $n_x \times n_y = (256)^2$ and $n_z = 8$ with a physical box dimension of $L_x = L_y = 128\rho_s$ in units of the drift scale.

The present computations represent the first results combining both warm ion and full

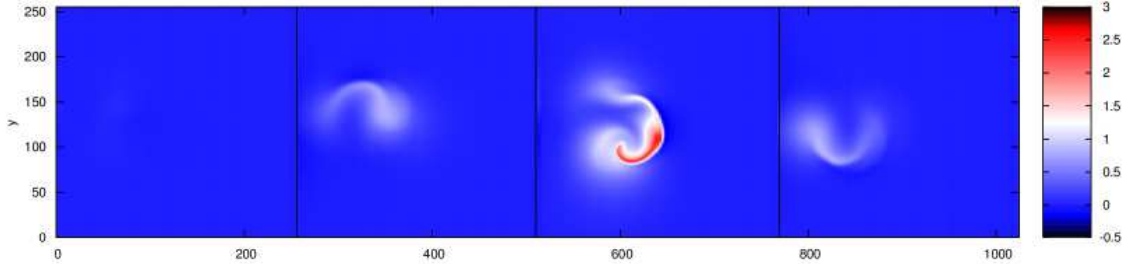


FIG. 2: *Electron density $n_e(x, y)$ filament (blob) at $t = 40$ for four of eight parallel sections ($z = 0$, $z = 2$, $z = 4$, $z = 6$) along the field line. The pronounced up-down asymmetry is caused by FLR and drift effects.*

3-d effects (electromagnetic, drift effects, and toroidal geometry) on scrape-off-layer blob motion. A relevant result concerning the main plasma blob motion itself is, that for the present scenario the τ_i and FLR effects slightly dominate the evolution of the blob structure compared to the drift effects. This result is of course strongly dependent on the specific parameters and will be discussed in more detail elsewhere. For the moment we are more interested in the proof-of-principle model for dynamical ionization by the blob front.

The evolution of the blob is here first followed until $t = 40$ in time units of c_s/L_\perp . For typical tokamak edge parameters this time corresponds to around $100 \mu\text{s}$.

In Fig. 2 the electron density $n_e(x, y)$ in the perpendicular (x, y) plane of the evolved blob is shown at $t = 40$ for four parallel sections ($z = 0$, $z = 2$, $z = 4$, $z = 6$) along the field line. In Fig. 3 only the $z = 4$ outboard midplane sections (with the strongest interchange drive by normal curvature) for the electron density and the Be impurity ion density are enlarged. Here the plume-like blob is propagating to the right into a neutral Be cloud.

The main plasma blob shows the characteristic plume-like form (similar to Rayleigh-Bénard convection), with pronounced up-down asymmetries caused by warm ion and drift effects. The beryllium ions form a more concentrated structure, which is determined by ionization at the blob front propagating into the radially inhomogeneous neutral cloud, and subsequent convection around the dipolar blob vortex. The densities $n(x)$ of electrons, ions and neutrals are shown (with different specific normalizations) in fig. 4 for $y = L_y/2$ for the same situation and time as in fig. 3 with different specific normalizations. The impurity ion profile is mainly determined by the overlap between the neutral cloud and the impacting blob.

This main result is similar for other dynamically ionized impurity species like helium

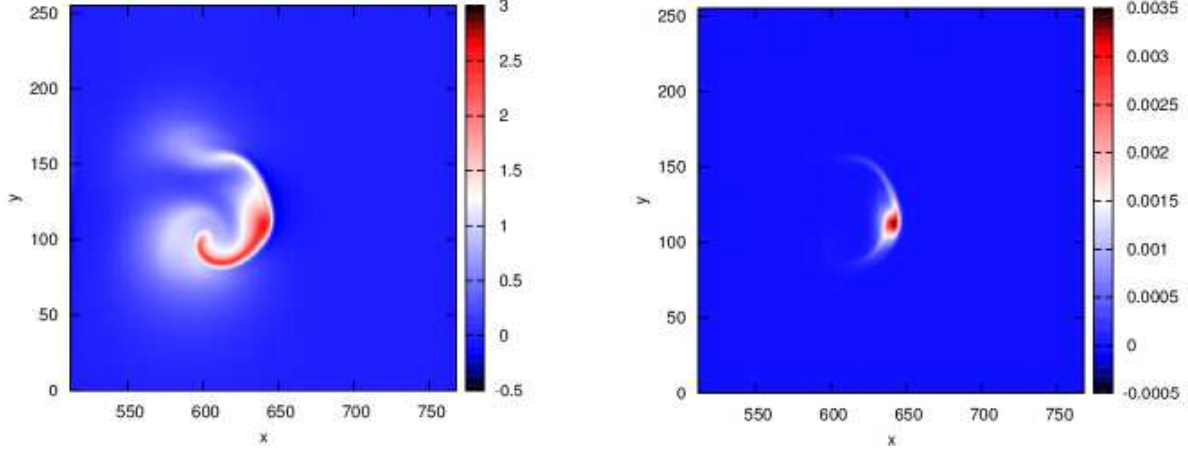


FIG. 3: *Left: electron density blob propagating to the right into and ionizing a neutral Be cloud (not shown); right: Be^+ impurity ion density; enlarged for only the outboard mid-plane section $z = 4$ of the computational domain.*

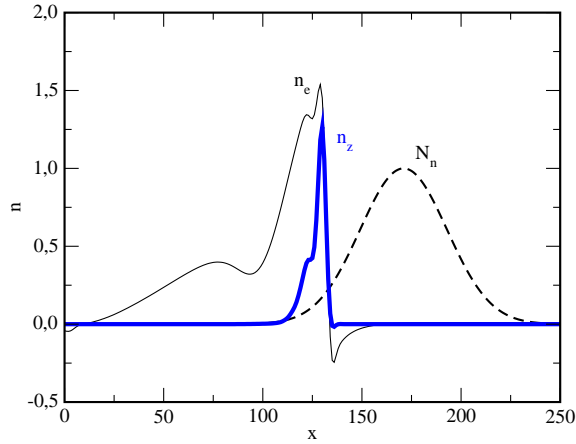


FIG. 4: *Radial profile of the electron, impurity and neutral densities (with different normalizations) at $y = L_y/2$ to illustrate the situation in fig.3.*

and carries significance for the interpretation of gas puff images which follow the spatio-temporal evolution of blobs. As a first step towards implementing a “virtual diagnostic” for He puff imaging of edge turbulence into the gyrofluid code, we plot in fig. 5, for the same blob parameters as above, the product of the electron density and helium ion density at time $t = 60$. This quantity is proportional to the recombination rate and thus is related (as a first approximation) to the optical emission of He. In order to separate the eventual effects of a localized impurity source we have in this case used a flat (constant) radial distribution of neutral helium.

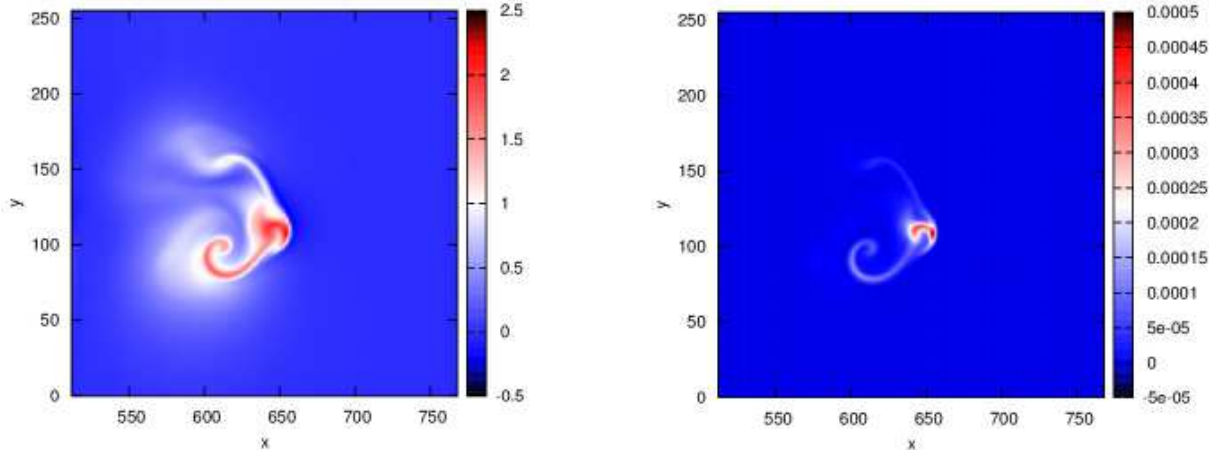


FIG. 5: *Left: electron density blob propagating to the right across a constant neutral helium source. Right: product $n_z \cdot n_e$ of the ionized He^+ impurity density with the electron density. Only the outboard mid-plane section $z = 4$ of the computational domain is shown.*

It is evident that the fast camera images delivered by imaging diagnostics in fusion experiments may not completely capture the whole actual blob structure if the gas puff is inhomogeneous. For a more realistic comparison 3-d averaging effects along the line of sight and camera angle will further have to be taken into account. Implementation of proper virtual diagnostics in turbulence code for interpretation of experimental SOL transport (and, vice versa, for experimental validation of the models and codes) is a relevant issue which has to be considered in the appropriate detail in future work.

V. TURBULENT INWARD TRANSPORT OF HYDROCARBON IONS

The next case is turbulence driven at the edge-core interface by a source of constant density flux, resulting in the formation of a turbulent (L-mode like) edge pedestal and subsequent transport of blob-like vortex structures into the SOL. The turbulence and profile are evolved until a saturated turbulent state is reached (here for $t > 1000$), where the average radial profiles (and energetic turbulence quantities) remain quasi stationary. We initialize a Gaussian neutral distribution around the right computational (wall) boundary and follow its ionization and the further net inward convection of the resulting impurity ions.

Parameters are $\hat{\epsilon} = 27000$, $\hat{\beta} = 1$, $\hat{C} = 3.5$, $\tau_i = 1$, and $\kappa_0 = 0.03$. We now consider the single ionization of ethylene as trace impurity species ($a_z = 0$, $\tau_z = 0$, $\mu_z = 14$) as specified

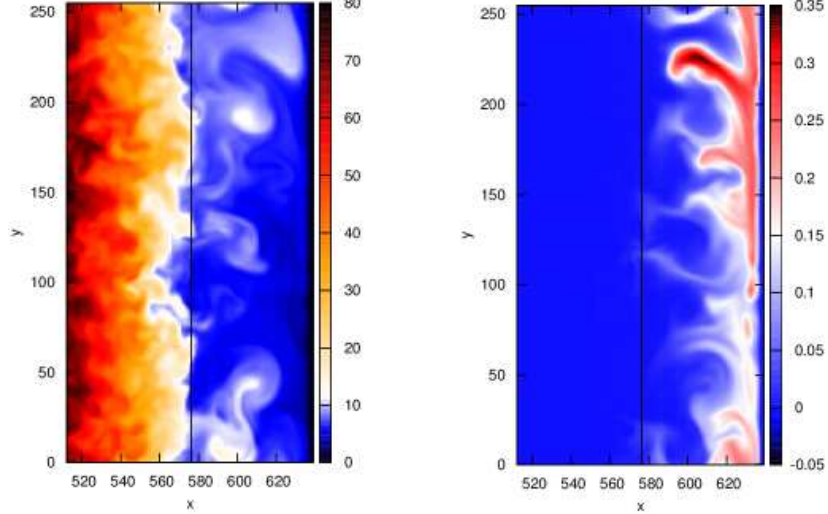


FIG. 6: *Left: Electron density $n_e(x, y)$ in a source flux driven turbulence computations including profile gradient evolution from the pedestal top (left boundary) across the separatrix (black middle line) into the scrape-off layer. Right: a wall-localized neutral ethylene cloud acts as source for electron-impact ionized $C_2H_4^+$ impurity ions density $n_z(x, y)$ which is further transported inwards.*

above. The computational dimensions in this case are set to $n_x \times n_y \times n_z = 128 \times 256 \times 16$ with $L_y = 256\rho_s$. For the given parameters normalized to typical ASDEX Upgrade edge conditions this corresponds to a box of approximately 5 cm width in the radial direction, centered around the last closed flux surface, and 10 cm length in the perpendicular direction.

Fig. 6 shows the electron density $n_e(x, y)$ at the left and impurity density $n_z(x, y)$ at the right at a snapshot in time $\Delta t = 40$ after switching on the neutral source. Only the outboard midplane section $z = 8$ of 16 parallel sections is here displayed. The impurities are rapidly advected inwards from the wall with some fingers already protruding into the closed field line region. After some time a more smoothly distributed radial impurity ion profile will form.

For illustration of the diffusive turbulent spreading of impurity ions from the SOL to the closed-field line edge region we prepare an additional case, where we inject an already pre-ionized cloud (again in the form of a radially localized Gaussian distribution) of trace impurities into the radial middle of the SOL domain and follow its average evolution for longer times.

Fig. 7 shows the time evolution of $\langle n_z(x) \rangle_{y,z}$ by its radial spreading at five times up to $\Delta t = 100$ after injection compared to the averaged radial profile of the electron density. The

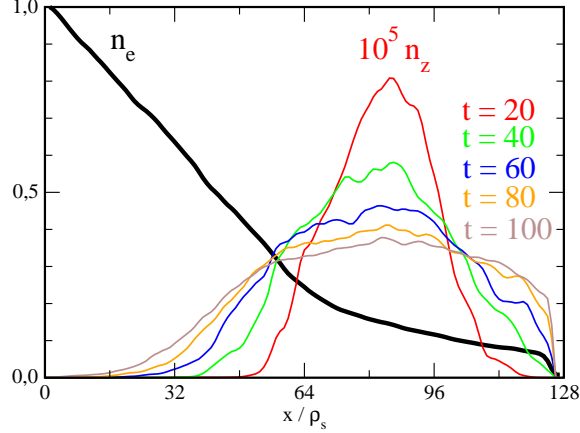


FIG. 7: Turbulent spreading of impurities initially localized in the SOL into the closed-field line main plasma region at various times after injection.

impurities rapidly spread across the separatrix (at $x = 64\rho_s$) into the main plasma region on a time scale of the order of cross-field blob propagation times.

A net pinch effect is not discernible in this figure, as the poloidal (z direction) initial impurity distribution is only weakly ballooned (i.e. extended over all z planes), and the plot shows the flux-surface averaged density, so that inward and outward curvature pinch effects (if present) mostly cancel. But also when the initial distribution is localized to the low-field side and only the y -average of $\langle n_z(x, z_0) \rangle_y$ at this position is taken, only a very slight inward pinch can be detected (by obtaining a quadratic fit of the logarithm of the averaged impurity density), which is however insignificant compared to the uncertainty present in the fit for times before the spreading becomes influenced by the outer radial boundary.

For a further discussion of impurity pinch effects in the SOL and edge region therefore better statistics would be necessary, by either strongly increasing the computational domain in the y direction (and thus getting a better y average), or by studying a large number of impurity puffs and taking additionally an ensemble average over the results. In any case the pinch effect here appears to be small compared to the (turbulent) diffusive spreading of the cloud.

VI. GAS PUFF IMAGING OF FILAMENTARY TURBULENT STRUCTURES

Now we take the Be ions out of the simulations and instead insert a helium gas puff localized radially in the centre of the SOL region, and take a snapshot after $\Delta t = 20$. We set up a virtual gas puff imaging (GPI) diagnostics while taking into account dynamical ionization effects on the initially neutral gas. The local emissivity of helium can be approximated by a power law dependence on electron density and temperature as $I \sim n_{n0} n_e^\alpha T_e^\beta$ with $\alpha \sim 0.4-0.6$ and $\beta \sim 0.6-0.8$ [44, 55–58]. A comparison of scrape-off-layer turbulence measured in Alcator C-Mod by probe and (deuterium) GPI diagnostics with three-dimensional gyrofluid computations has recently been carried out by Zweben and Scott et al. [55] using the 6-moment code GEMR. There the neutral gas density n_{n0} has been assumed to be constant in space and time over the computational area of interest. The GEMR computations, which also evolve temperature dynamics, further showed that the fluctuating electron temperature is closely correlated to the electron density [55], so that the emissivity may here be well approximated as $I \sim n_{n0} n_e^{\alpha+\beta}$.

However, the neutral gas cloud density $n_{n0}(x)$ may get dynamically reduced by local electron impact ionization from impinging turbulent blobs. We here take this effect into account, which strongly depends on the specific plasma parameters in the SOL. The neutral gas density is reduced in time as

$$\partial_t n_n = -n_n n_e R(T) \equiv -\hat{\omega}_R n_n. \quad (11)$$

The constant parameter R_0 in eq. (8) is about $R_0 \approx 4 \cdot 10^{-9} \text{ cm}^3/\text{s}$ when the temperature enters in units of eV and the cross section is given in units of 10^{-16} cm^2 . The magnitude of $R(T)$ for helium is in the order of R_0 for typical near-separatrix SOL temperatures (of around 10-20 eV). If we assume a corresponding electron density of around $n_e \sim 10^{13} \text{ cm}^{-3}$ then the combination $\omega_R \equiv n_e \cdot R \sim 10^4 - 10^5 \text{ 1/s}$. In drift normalized units $\hat{\omega}_R = \omega_R L_\perp / c_s$. For a SOL gradient scale length of $L_\perp = 2 \text{ cm}$ and $T_e = 20 \text{ eV}$ in deuterium plasma we thus have a time scale of $L_\perp / c_s \sim \mu\text{s}$, and arrive at an (order of magnitude) estimate of $\hat{\omega}_R \approx 10^{-2} - 10^{-1}$ for the drift normalized reduction rate.

In fig. 8 we plot the electron density (top left) and the spatial distribution of the simulated GPI emission intensity for various values of the neutral (helium) reduction rate: $\hat{\omega}_R = 0$ (top right), $\hat{\omega}_R = 0.2$ (bottom left), $\hat{\omega}_R = 0.5$ (bottom right). The results show that not only the intensity but also the spatial structure of the emission strongly depends on the plasma

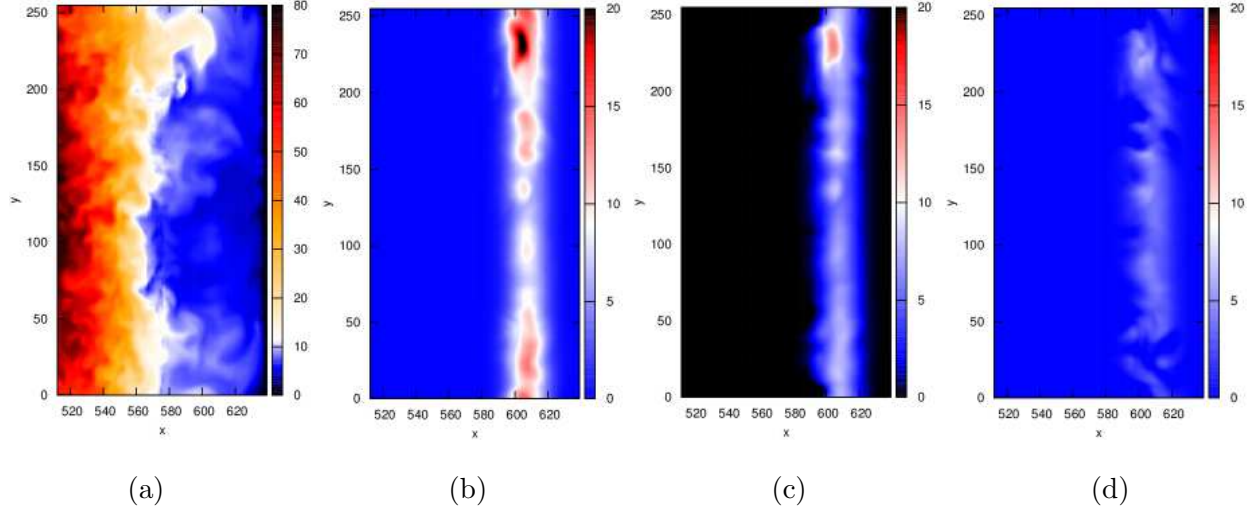


FIG. 8: A radially localized neutral helium gas cloud $n_{n0}(x)$ is puffed into the middle of the SOL and dynamically ionized by electron impact. (a) On top left a snapshot of the turbulent background electron density $n_e(x, y)$ at time $\Delta t = 20$ after injection is shown. The local instantaneous emission $I(x, y) \sim n_{n0}n_e^{\alpha+\beta}$, simulating a virtual GPI diagnostic, is shown for three values of the neutral depletion rate: (b) $\omega_R = 0$, (c) 0.2 and (d) 0.5.

parameters: for low electron densities the impact ionization rate is small, and over typical turbulent or blob time scales no significant effect is visible. The image for $\hat{\omega}_R = 0.01$ is indistinguishable from the one for $\hat{\omega}_R = 0$. For larger SOL densities and thus larger $\hat{\omega}_R > 0.1$ the dynamical ionization may however distort the obtained GPI picture.

A common caveat concerning both the GEMR code and our code is the use of local “delta-f” models, which is strictly only applicable radially locally in thin layers of plasma. In a global sense the “delta-f” condition of small fluctuation amplitudes compared to the background is never really fulfilled for typical SOL conditions. More realistic 3-d gyrofluid code comparisons with SOL measurements in future have to be based on “full-f” global edge-SOL models, which are presently still under development [59].

VII. CONCLUSIONS

We have shown how measured and calculated electron impact ionization cross section data can be included in multi-species gyrofluid modelling of turbulence in the edge of magnetized fusion plasmas. Here exemplarily only one trace impurity species in addition to the main plasma species has been implemented. In principle any number of further impurities or charge states can be straightforwardly added. A number of restrictions of the model remain to be resolved before any detailed realistic comparison between the gyrofluid code results and actual measurements in the SOL of tokamaks may be undertaken. The most important generalization to the present models will be development of 3-d 6-moment multi-species “full-f” codes including fully global evolution of the turbulence and profiles. In such a model also the back reaction of (non-trace) impurities on local turbulence and flow structure could be consistently included. Further care will have to be devoted to the implementation of realistic flux surface geometry including a consistent treatment of the X-point and separatrix.

Acknowledgements

This work is dedicated to Tilmann Märk on the occasion of his 70th Birthday Honor Issue of the International Journal of Mass Spectrometry. The work was partly supported by the Austrian Science Fund (FWF) Y398, and by the European Commission under the Contract of Association between EURATOM and ÖAW, carried out within the framework of the European Fusion Development Agreement (EFDA). The views and opinions expressed herein do not necessarily reflect those of the European Commission.

-
- [1] G. Janeschitz et al., *Journal of Nuclear Materials* **290-293**, 1 (2001).
- [2] G. Federici, P. Andrew, P. Barabaschi, et al., *Journal of Nuclear Materials* **313-316**, 11 (2003).
- [3] J. Roth, E. Tsrtrone, A. Loarte, et al. *Journal of Nuclear Materials* **390-391**, 1 (2009).
- [4] R.E.H. Clark, D.H. Reiter (eds.): *Nuclear fusion research - understanding plasma-surface interactions*. Springer, Berlin 2005.
- [5] W.M. Tang, *Nucl. Fusion* **18**, 1089 (1978).
- [6] J. Hugill, *Nucl. Fusion* **23**, 331 (1983).
- [7] P.C. Liewer, *Nucl. Fusion* **25**, 543 (1985).
- [8] A.J. Wootton, B. A. Carreras, H. Matsumoto, et al., *Phys. Fluids B* **2**, 2879 (1990).
- [9] A.M. Dimits, G. Bateman, M. A. Beer, et al., *Phys. Plasmas* **7**, 969 (2000).
- [10] B.D. Scott, *Plasma Phys. Contr. Fusion* **45** A385 (2003).
- [11] X. Garbet, P. Mantica, C. Angioni, et al. *Plasma Phys. Controlled Fusion* **46**, B557 (2004).
- [12] G.R. Tynan, A. Fujisawa, and G. McKee, *Plasma Phys. Control. Fuson* **51**, 113001 (2009).
- [13] P H. Diamond, S.I. Itoh, K. Itoh, and T.S. Hahm, *Plasma Phys. Controlled Fusion* **47**, R35 (2005).
- [14] A. Kendl, B. Scott and T.T. Ribeiro, *Phys. Plasmas* **17**, 072302 (2010).
- [15] B.D. Scott, *Phys. Plasmas* **12** 102307 (2005).
- [16] T.T. Ribeiro and B.D. Scott, *Plasma Phys. Control. Fusion* **47** 1657 (2005).
- [17] T.T. Ribeiro and B.D. Scott, *Plasma Phys. Control. Fusion* **50** 055007 (2008)
- [18] B.D. Scott, *Phys. Plasmas* **5** 2334 (1998).
- [19] B.D. Scott, *Phys. Plasmas* **8** 447 (2001).
- [20] G.E. Karniadakis, M. Israeli, S.A. Orszag, *J. Comput. Phys.* **97**, 414 (1991).
- [21] A. Arakawa, *J. Comput. Phys.* **1**, 119 (1966).
- [22] V. Naulin, A. Nielsen, *SIAM J. Sci Comput.* **25**, 104 (2003).
- [23] G.L. Falchetto, B.D. Scott, P. Angelino, et al., *Plasma Phys. Control. Fusion* **50**, 124015, 12pp (2008).
- [24] J. Madsen, O.E. Garcia, J.S. Larsen, et al., *Phys. Plasmas* **18**, 112504 (2011).
- [25] V. Naulin, *Phys. Rev. E* **71**, 015402 (2005).

- [26] M. Priego, O.E. Garcia, V. Naulin, J.J.Rasmussen, Phys. Plasmas **12**, 062312 (2005).
- [27] N. Dubuit, X. Garbet, T. Parisot et al, Phys. Plasmas **14**, 042301 (2007).
- [28] S. Futatani, D.del-Castillo-Negrete, X. Garbet et al., Phys. Rev. Lett. **109**, 185005 (2012).
- [29] H. Deutsch and T.D. Märk, Int. J. Mass Spectrom. Ion Proc. **79**, R1 (1987).
- [30] H. Deutsch, K. Becker, T.D. Märk, Contrib. Plasma Phys. **35**, 421 (1995)
- [31] H. Deutsch, K. Becker, M. Probst, T.D. Märk, Advances in Atomic, Molecular and Optical Physics **57**, 87 (2009).
- [32] K.Becker, F.Biasioli, G.Denifl, et al., NIST Special Publications, **926**, 205-209 (1988).
- [33] T.D. Märk, Plasma Phys. Control. Fusion **34**, 2083 (1992).
- [34] S.H. Müller, C. Holland, G.R. Tynan, J.H. Hu and V. Naulin, Plasma Phys. Control. Fusion **51**, 105014 (2009)
- [35] T. Maihom I. Sukuba, R. Janev, et al., Eur. Phys. J. D. **67**, 2 (2013).
- [36] K. Gluch, P. Scheier, W. Schustereder, et al., Int. J. Mass Spectrom. **228**, 307 (2003).
- [37] S. Feil, K. Gluch, A. Bacher, et al., J. Chem. Phys. **124**, 214307 (2006).
- [38] N. Endstrasser, F. Zappa, A. Mauracher, et al., Int. J. Mass Spectrom. **280**, 65 (2009).
- [39] S. Feil, A. Bacher, K. Gluch, et al., Int. J. Mass Spectrom. **253**, 122 (2006).
- [40] S.E. Huber, J. Seebacher, A. Kendl and D. Reiter, Contrib. Plasma Phys. **51**, 931 (2011).
- [41] D. Reiter and R.K. Janev, Contrib. Plasma Phys. **50** 986 (2010).
- [42] D. Reiter and B. Küppers, <http://www.hydkin.de> (2010).
- [43] A. Kallenbach, M. Bernert, R. Dux, et al. *Impurity seeding for tokamak power exhaust: from present devices via ITER to DEMO*, Plasma Phys. Contr. Fusion (2014), in print.
- [44] R.J. Maqueda, G.A. Wurden, D.P. Stotler et al., Rev. Sci. Instrum. **74**, 2020 (2003).
- [45] K.L. Bell, H.B. Gilbody, J.G. Hughes, et al., L. Phys. Chem. Ref. Data **12**, 891 (1983).
- [46] Y. Ralchenko, R. Janev, T. Kato et al., Atomic and Nuclear Data tables **94**, 603 (2008).
- [47] S.I. Krasheninnikov, Phys. Lett. A **283**, 368 (2001).
- [48] G.Q. Yu and S.I. Krasheninnikov, Phys. Plasmas **10**, 4413 (2003).
- [49] O.E. Garcia, V. Naulin, A.H. Nielsen and J.J. Rasmussen, Phys. Rev. Lett. **92**, 165003 (2004).
- [50] O.E. Garcia, N.H. Bian and W. Fundamenski, Phys. Plasmas **13**, 082309 (2006)
- [51] O.E. Garcia, Plasma and Fusion Research **4**, 019 (2009).
- [52] J.R. Angus, M.V. Umansky, and S.I. Krasheninnikov, Phys. Rev. Lett. **108**, 215002 (2012).
- [53] J.R. Angus, M.V. Umansky, and S.I. Krasheninnikov, J. Nucl. Materials **438**, S572 (2013).

- [54] J.R. Myra, W.M. Davis, D.A. D'Ippolito et al., Nucl. Fusion **53**, 073013 (2013).
- [55] S.J. Zweben, B.D. Scott, J.L. Terry et al., Phys. Plasmas **16**, 082505 (2009).
- [56] D.A. Russell, J.R. Myra, D.A. D'Ippolito, et al., Phys. Plasmas **18**, 022306 (2011).
- [57] I. Shesterikov, Y. Xu, M. Berte, et al., Review of Scientific Instruments **84**, 053501 (2013).
- [58] L.M. Shao, G.S. Xu, S.C. Liu, et al. Plasma Phys. Control. Fusion **55**, 105006 (2013)
- [59] J. Madsen, Phys. Plasmas **20**, 072301 (2013).